Title
Characterization of arterial plaque composition with dual energy computed tomography: a simulation study

Journal
The International Journal of Cardiovascular Imaging, 37(1)

ISSN
1569-5794

Authors
Ding, Huanjun
Wang, Chenggong
Malkasian, Shant
et al.

Publication Date
2021

DOI
10.1007/s10554-020-01961-y

Peer reviewed

HHS Public Access

Author manuscript

Int J Cardiovasc Imaging. Author manuscript; available in PMC 2022 January 01.

Published in final edited form as:

Int J Cardiovasc Imaging. 2021 January ; 37(1): 331–341. doi:10.1007/s10554-020-01961-y.

Characterization of arterial plaque composition with dual energy computed tomography: a simulation study

Huanjun Ding, **Chenggong Wang**, **Shant Malkasian**, **Travis Johnson**, **Sabee Molloi**

Department of Radiological Sciences, University of California, Irvine, California, 92697

Abstract

To investigate the feasibility of quantifying the chemical composition of coronary artery plaque in terms of water, lipid, protein, and calcium contents using dual-energy computed tomography (CT) in a simulation study. A CT simulation package was developed based on physical parameters of a clinical CT scanner. A digital thorax phantom was designed to simulate coronary arterial plaques in the range of 2–5 mm in diameter. Both non-calcified and calcified plaques were studied. The non-calcified plaques were simulated as a mixture of water, lipid, and protein, while the calcified plaques also contained calcium. The water, lipid, protein, and calcium compositions of the plaques were selected to be within the expected clinical range. A total of 95 plaques for each lesion size were simulated using the CT simulation package at 80 and 135 kVp. Half-value layer measurements were made to make sure the simulated dose was within the range of clinical dual energy scanning protocols. Dual-energy material decomposition using a previously developed technique was performed to determine the volumetric fraction of water, lipid, protein, and calcium contents in each plaque. For non-calcified plaque, the total volume conservation provides the third constrain for three-material decomposition with dual energy CT. For calcified plaque, a fourth criterion was introduced from a previous report suggesting a linear correlation between water and protein contents in soft tissue. For non-calcified plaque, the root mean-squared error (RMSE) of the image-based decomposition was estimated to be 0.7%, 1.5%, and 0.3% for water, lipid, and protein contents, respectively. As for the calcified plaques, the RMSE of the 5 mm plaques were estimated to be 5.6%, 5.7%, 0.2%, and 3.1%, for water, lipid, calcium, and protein contents, respectively. The RMSE increases as the plaque size reduces. The simulation results indicate that chemical composition of coronary arterial plaques can be quantified using dual-energy CT. By accurately quantifying the content of a coronary plaque lesion, our decomposition method may provide valuable insight for the assessment and stratification of coronary artery disease.

Keywords

Dual energy; CT; plaque; material decomposition

The authors have no relevant conflicts of interest to disclose.

1. Introduction

A significant amount of work has been done on the algorithms and clinical applications of material decomposition using dual energy computed tomography (CT) [1–7]. Dual energy CT decomposition has successfully been used to quantify bone mineral density. Alvarez *et al.* [8] reported the ρZ method in pre-construction (projection) space for dual energy CT material decomposition. Lehmann *et al.* [9] reported the basis material method for dual energy material decomposition. Fundamentally, the ρZ method is equivalent to the basis material method. However, the basis material decomposition method is more practical in clinical applications since it can determine the mass fraction of two materials in a mixture or compound of interest directly, as well as the effective density and effective atomic number, while the ρZ method only gives the effective density and effective atomic number of the whole mixture. Those decomposition methods were limited to a two-material mixture, which limited the clinical application of the dual energy CT decomposition [10, 11].

Recently, the performance of the dual energy CT has been improved in terms of both basic technology and new clinical applications. Different materials have different mass attenuation coefficients when interacting with X-rays, which is how dual-energy imaging is able to quantify material compositions in a region of interest. Therefore, in CT imaging, different tissue may be represented with either different or the same CT numbers depending on their chemical concentration. The National Institute of Standards and Technology (NIST) website supplies the mass attenuation coefficients for different elements (Z=1–92) [12]. It lists the coefficients of 48 compounds and mixtures, which include nearly all the chemical elements and compounds or mixtures found in the human body. For a mixture with more than one constituent element, the summation of weighted mass attenuation coefficients of each constituent element could generate the mass attenuation coefficient of the mixture.

Liu *et al.* [13] recently reported dual energy CT could successfully resolve a three-material mixture consisting of water, calcium hydroxyapatite and iron nitrate in a single voxel. A three-material decomposition dual energy CT algorithm, based on conservation of mass, was reported. They used a mixture composed of water, iron, and calcium, where the latter two materials were high Z materials with higher attenuation coefficients.

Dual energy CT has previously been used as one of the methods to diagnose coronary artery disease (CAD), especially to distinguish stable and unstable plaque [7, 14–16]. The use of dual-energy material decomposition in assessing coronary arterial plaque is mainly limited by two factors. First, coronary arterial plaques are usually composed of three to four materials; current algorithms cannot decompose mixture with four materials. Second, the size of the coronary arterial plaque is relatively small with an approximate range of 2–5 mm in diameter [17]. Partial volume effect makes quantitative measurements challenging [18]. In this case, the quantitative compositional analysis for a four-material mixture in a small-size arterial plaque is clinically important, as compositional analysis can potentially be used to decide whether it is a vulnerable plaque [19–21].

Coronary plaques are usually composed of three to four different materials, such as water, lipid, protein and sometimes calcium. The mass attenuation curves for water, lipid, protein,

and calcium are shown in Figure 1. The mean attenuation coefficient of calcium is higher than that of water, lipid and protein for much of the diagnostic energy range (~33 – 80 keV). Because of this, calcium is easily discerned from other mixture components. Conversely, water, lipid, and protein are difficult to differentiate in mixtures, as their attenuation coefficients are very similar.

The primary goal of this study was to simulate the performance of three-material and four-material decomposition by using dual-energy CT, specifically, in the case where the region of interest is assigned to be a four-material mixture.

2. Theory

The decomposition of measured linear attenuation into fractional measurements of tissue composition was based on the solution to a dual energy system of three equations and three unknowns:[22, 23]

$$\begin{cases} \mu_W^L \cdot f_W + \mu_L^L \cdot f_L + \mu_{Ca}^L \cdot f_{Ca} = S^L \\ \mu_W^H \cdot f_W + \mu_L^H \cdot f_L + \mu_{Ca}^H \cdot f_{Ca} = S^H \\ f_W + f_L + f_{Ca} = 1 \end{cases} \quad (1)$$

where μ_W^i, μ_L^i, and μ_{Ca}^i are the linear attenuation coefficients of water, lipid, and calcium, respectively, where i denotes either low (L) or high (H) energy scans. f_W, f_L, and f_{Ca} are the volume fractions of water, lipid, and calcium, respectively. S^L and S^H are the measured CT Hounsfield units (HU) for the low and the high-energy scans, respectively. The first two equations represent the measured log signal in the low or high energy scan, as a linear combination of the attenuation coefficients of the three components, while the last equation comes from the CT voxel size constraint [1, 23–25]. The assumption of mass conservation would be more universal. However, it requires the knowledge of the exact incidence spectra from the X-ray source, which can be difficult to obtain in practice. One of the first descriptions of the use of the dual energy CT with 3 equations and 3 unknowns to solve for the soft tissue, fat and bone composition of spongiosa was first introduced by Goodsitt *et. al.* in 1987 [26]. Conversely, for soft tissue components such as water, lipid, and protein, the errors induced by the assumption of volume conservation can be negligible [1, 22, 23].

Although the theory of dual energy imaging is well represented in Eq. 1, some technical obstacles remain due to the use of polyenergetic spectra and the presence of the non-linear artifacts. Instead of solving Eq. 1 directly, low-order polynomial approximations are usually used for generating the basis images from the measured signals [8, 9]. In this study, we chose a non-linear equation with the following form to approximate the inverse of Eq. 1:

$$f_i = \frac{a_0 + a_1 S^L + a_2 S^H + a_3 (S^L)^2 + a_4 S^L S^H + a_5 (S^H)^2}{1 + b_1 S^L + b_2 S^H} \quad (2)$$

where f_i stands for f_W, f_L, and f_{Ca}. Solving for f_W, f_L, and f_{Ca} was a two-step process that was accomplished numerically by means of least-squares fitting. The first step was

substituting the known values and each respective image attenuation measurement of f_W, f_L, and f_{Ca} from the calibration phantom. Origin (OriginLab Co., Northampton, MA) was used to perform the non-linear fitting according to Eq. 2 and solve for the system matrix calibration coefficients, a_0, a_1, a_2, a_3, a_4, a_5, b_1, and b_2 for each material, respectively. After determining these coefficients, image attenuation measurements from vessels with unknown compositions were substituted into the system to determine the image-based measurements of water, lipid, and calcium contents [22].

3. Method

a. CT simulation

The current simulation study was designed to match the physical parameters of a specific CT scanner (Canon Aquilion One, Canon America Medical Systems, Tustin, CA) as close as possible, so that it may bring more useful information for the future phantom studies. Polyenergetic x-rays were simulated within the range of 80 – 135 keV. Spectra was provided by the XCOMP5R code of Nowotny and Hoofer [27]. The polyenergetic x-ray beam flux at 80 and 135 kVp tube voltage is shown in Fig. 2. We chose the aluminum pre-filtration of the low- and high- energy beams to make sure they could match the mean beam energies of 53.3 and 71.0 keV for the physical CT scanner at tube voltages of 80 and 135 kVp, respectively. By incrementally increasing the thickness of aluminum until the desired mean beam energies were reached, a total added filtration of 7.5 mm aluminum was selected in the current simulation study. The half-value layer of each reference beam was determined to be approximately 5.35 mm Al and 8.53 mm Al for the 80 kVp beam and the 135 kVp beam, respectively. The amount of the aluminum filtration did not change throughout the study regardless of which tube voltage we used. Although some scanners use different filtrations for the low- and high-energy beam to improve spectral separation, Canon Aquilion One, which is the modeled CT scanner in this simulation study, does not switch filtration between different kVps. The presence of a bowtie filter was not simulated in the current study. Sinograms were simulated using ray tracing method, realized through the ASTRA Toolbox in MATLAB [28]. Quantum noise was introduced using Poisson noise model in the sinogram to reflect the realistic dose level. Focal spot blurring was introduced with a Gaussian filter on the sinogram, which matched the 0.9 mm focal spot size in the physical scanner. Simulated CT images were reconstructed with Filtered Back Projection (FBP) using a Ram-Lak filter. Based on the simulation parameters, the estimated $CTDI_{vol}$ from the Canon Aquilion One CT scanner were calibrated to be 18.9 and 22.1 mGy for 80 and 135 kVp, respectively. The detailed parameters used in the simulation are summarized in Table 1.

b. Phantom design

A 3200×2200 pixel ordinal digital phantom was created to emulate an axial cross-sectional CT image of a 32-cm wide human chest, with four vessels located along the anterior edge of the simulated heart and 0.01 cm/pixel resolution. The size of the lesions used in simulation was in the range of 2–5 mm diameter. For compositions, we used the range of water, lipid, protein and Ca according to expected clinical range. Although the calcification in the plaque is calcium hydroxyapatite rather than Ca, we have carefully converted the Ca volumetric fraction according to the mass ratio of Ca in hydroxyapatite. In this case, the amount of Ca

used in the simulation is clinically relevant. We generated random numbers within the range for water and Ca volumetric fraction. We determined the protein volumetric fraction using the assumed linear correlation between water and protein with a random Gaussian noise addition. We finally determined the lipid volumetric fraction by assuming the sum of the all components is 1. Materials were assigned indices according to the chest phantom shown in Figure 3, and X-ray attenuation coefficients for each material were derived using data from NIST. The white objects were designed to simulate the ribs and vertebra in the body. The central circle was used to simulate the area of heart. Two designated regions in the left and right lung tissue stand for the air and water regions used to calibrate Hounsfield Units, in each simulation.

The soft tissue of arterial plaque consists of a fibrous cap and fatty core. The fatty tissue contains mostly lipid, while the fibrous cap consists of water, lipid, and protein. Therefore, there exists a biological correlation between water and protein, as both contents appear primarily in the same type of tissue. This assumption has been demonstrated in a previous study on breast tissue [29]. For arterial plaque, the correlation coefficients may be different but the concept is expected to be similar. The assumption that there is a biological correlation between water and protein renders the possibility of decomposing arterial plaque into four basis materials.

To make the simulation more realistic, Gaussian noise was introduced to the linear relationship in the previously reported data [29], yielding data shown in Figure 4. We used the linear relationship in Figure 4 to decompose the protein content from the four-material mixture.

Table 2 shows the mixture composition we used in the simulation. Generally, coronary plaques were classified into calcified and non-calcified plaques [30]. The calcified plaque contains water, lipid, protein, and calcium while the non-calcified plaque contains only water, lipid, and protein. Previously reported plaque compositions are also included in Table 2 [31, 32]. The column labeled, “simulation” represents the mixture of contents we used in our simulation. In order to make the simulation more realistic, the plaque compositions were chosen to be within the previous reported range.

c. Simulation and material decomposition calibration

A digital circular phantom was designed for the dual-energy calibration purposes. The calibration phantom had a diameter of 30 cm, with four 5 cm circular plugs. The background material was assigned as PMMA, and each of the four plugs was simulated as known mixtures of water, lipid, protein, and Ca. CT images of the calibration phantom was simulated using our CT simulation package. The compositions of the four plugs were modified each time to generate a total of 22 calibration points. The simulated HU of the low- and high-energy CT images of those calibration points were substituted into Eq. 2 (S^L and S^H), together with the known fraction of the content (f_i), so that the decomposition coefficients of the corresponding content (a_i and b_i) could be determined. Those decomposition coefficients were used later in the validation study with the simulated low- and high-energy HU to derive the composition of the plaque. For calcified plaques, the same technique was first used to decompose the tissue into each component. However, due to the

presence of four different components in the plaque, the decomposed values may not reflect the true volumetric percentages. Therefore, a secondary calibration was required. To address this issue, a linear transformation of the initial results from the dual-energy decomposition was performed to obtain the final volumetric percentages. The slope and the offset of this linear transformation were determined from a linear fitting of 10 samples with known chemical volumetric fractions.

d. Validation and image analysis

Ninety- five different vessel percent volume compositions were simulated during each trial, as determined by a clinically constrained material distribution for water, lipid, protein, and calcium. For each trial, 47 pairs of simulated images were created. Two different vessel compositions of water, lipid, protein, and calcium were assigned to Vessel Group 1 and Vessel Group 2, according to Figure 3, for each image pair. In this case, each mixture was simulated on both the left and right vessels and the location effect on the mixture decomposition could be studied. While one image of the pair was simulated with 80 kVp and 218.4 mA, the other image was simulated with 135 kVp and 65.6 mA. The tube current was adjusted to achieve the same radiation dose for the low and high energy images. In this simulation study, we adjusted our simulation dose to be similar to the typical clinical dose. We used 218 mA at 80 kVp with a dose of 19 mGy and 65 mA at 135 kVp with a dose of 23 mGy. The previously reported dose for dual energy CT scan is 20 mGy at 80 kVp and 23 mGy at 135 kVp [33, 34]. Therefore, the current simulation study was done within the clinically acceptable dose range. The mean HU of each vessel in the simulated image was calculated using a region of interest of approximately 50% of the luminal area of the vessel in order to minimize the partial volume effects.

Five simulation trials were conducted where vessel lumen cross-sectional images were simulated. The details of the trials are shown in Table 3. In Trial 1, non-calcified plaques were simulated with 2 mm vessels, which consisted of mixtures of water, lipid, and protein contents. In Trial 2, calcified plaques were simulated with 5 mm vessels, which consisted of mixtures of water, lipid, protein, and calcium contents. The protein volumetric fractions in this data set were directly correlated to those of water without any correlation noise. Trial 3 had the same design as Trial 2, but with added Gaussian noise in the water-protein correlations when the plaque composition was determined for the digital phantom. It is thus demonstrated the effect of uncertainty in this biological correlation. In Trials 4 and 5, simulated vessel diameters were reduced to 3 and 2 mm, respectively. Vessel compositions for Trials 4 and 5 were simulated with added Gaussian noise in the water-protein correlations to include the biological uncertainty as well.

e. Statistical analysis

In this study, we used the linear regression model to fit our decomposition data to conduct the statistical analysis. Slopes from the linear fitting between the measured and the known volumetric fractions were used to investigate the correlation of the results.

We calculated the RMSE to determine the accuracy of our decomposition studies. RMSE is frequently used to measure the differences between values observed and the value predicted

by a model or an estimator. RMSE is an accuracy measurement, which is used to compare forecasting errors of different models for a particular variable. It did not compare between variables so it is scale-dependent.

We also calculated the standard error of estimate (SEE) to determine the precision of our decomposition studies. The standard error of the estimate is a prediction accuracy measurement. We used the regression line to minimize the sum of squared deviations of prediction. The standard error of the estimate is defined below:

$$\sigma_{est} = \sqrt{\frac{\sum (Y - Y')^2}{N}} \tag{4}$$

Where σ_{est} the standard error of the estimate, N is the number of pairs of scores, Y is an actual score and Y' is a predicted score. The sum of squared differences between the actual scores and the predicted scores is the numerator.

4. Results

The results of the tissue composition measurements of the non-calcified plaques are presented in Fig. 5 for water (a), lipid (b), and protein (c) contents. The volumetric fractions of the three components measured with the image-based dual energy technique were compared to the known contents. The identity lines are shown in each plot for visual clarity. The correlation between the image-based measurement and the designed one was estimated with a linear regression model. The fitted slopes were estimated to be 1.01, 1.09, and 1.01 for water, lipid and protein contents, respectively. The RMSE of the image-based decomposition with respect to the known volumetric fraction is estimated to be 0.7%, 1.5%, and 0.3% for water, lipid, and protein contents, respectively. The linear regression results show a good agreement between the measured and the known compositions for all the vessels. The RMSE of lipid is slightly higher than those of water and protein. This is mostly due to the fact that the volumetric fraction of lipid is generally the highest among all chemical components in tissue.

Figure 6 shows the four- materials mixture decomposition results for calcified coronary plaques for water (a), lipid (b), calcium (c), and protein (d) contents. The volumetric fractions of the four components measured with the image-based dual-energy technique were compared to the known components. The identity lines are shown in each plot for visual clarity. The correlation between the image-based measurement and the known volumetric fraction was estimated with a linear regression model. The fitted slopes were estimated to be 0.97, 0.97, 1.00, and 0.92 for water, lipid, calcium, and protein contents, respectively. The RMSE of the image-based decomposition with respect to the known values from the designed mixture were estimated to be 5.6%, 5.7%, 0.2%, and 3.1% for water, lipid, calcium, and protein contents, respectively. The linear regression results show a good agreement between the measured and the known compositions.

Another interesting question is the location dependence for the quantitative plaque characterization. To investigate this issue, we studied the correlation of the image-based composition measurements from the left and right vessels of the same contents. This

correlation is shown in Figure 7 for the results obtained from dual energy decomposition (a) water, (b) lipid, (c) protein, and (d) calcium, respectively. The identity lines are shown in red for visual guidance. It can be seen from the dual-energy analysis that the image-based decomposition has good linear correlation, with a slope of 1.00, 1.00, 1.08, and 1.00 for the water, lipid, protein, and calcium, respectively, between the left and the right vessels.

The RMSE for different vessels is shown in Table 4. First, we compared the decomposition results for the Trial 2 and 3 (5 mm diameter vessels without and with noise) in the relationship of water and protein. We found that there is no obvious different between the RMSE for the Trial 2 and 3. However, we still observed that the RMSE for the decomposition results with added noise is slightly higher than the one without noise. Therefore, introduced noise in the correlation between the water and protein will affect the accuracy of our decomposition but the effect is limited, meaning our decomposition method is relatively independent of the noise. Compared to the range of the water, lipid, calcium, and protein, the RMSE for water, lipid, calcium, and protein is much smaller than the corresponding range, indicating that our decomposition results are very reliable. Knowing the noise introduced in the correlation between the water and protein would not affect the decomposition very much, we tested the four-material mixture decomposition in Trial 4 (3 mm diameter) and Trial 5 (2 mm diameter) vessels with random noise in the water-protein correlation. The RMSE of water, lipid, and protein for Trial 4 are approximately 50% higher than the ones of Trial 3. This is most probably due to the smaller vessels leading to partial volume effect. The measurement of image-based ROI is not strictly accurate and it affects the decomposition results. We also noticed that the RMSE of calcium in Trial 4 is close to the one for Trial 2. This is due to the higher Z number of calcium leading to the higher attenuation affect, which will be easier to distinguish among the water, lipid, and protein. As for the RMSE for Trial 5 for water, lipid, calcium, and protein, we observed that the RMSE number for four contents are almost the same as the trial 4 numbers, meaning that with the vessel diameter further decreasing, the four-material decomposition reached its limit but still has reliable results.

The standard error of estimation (SEE) on different vessels is shown in Table 5. The standard error of the estimate is a measure of the precision for predictions made with a regression line. The results show that for the 5 mm diameter vessels (Trial 2 and 3), the SEE value without the introduced noise is slightly lower than the one with noise, which is expected. The SEE for Trial 4 (3 mm diameter) and trial 5 (2 mm diameter) is nearly 50% higher than that of Trial 3, which indicates that the partial volume effect plays an important role for smaller vessels.

5. Discussion

Previous reports have shown that dual-energy CT material decomposition could be used for quantitative measurement in approximately 10 mm vessels for three high Z materials [13]. The current study investigated the possibility of dual-energy material decomposition in a 2 mm vessel with 3–4 different low Z materials. For the presence of three materials, i.e. water, lipid and protein contents, dual-energy material decomposition was accomplished by assuming total volume conservation in the current simulation study. Volume conservation is

a first order approximation and has been used successfully in previous studies [1, 22–25, 35]. Although total volume conservation may not always be true, it should be noted that the errors can be reasonably small in cases where the mass densities of the components and the effective density of the mixture are close to each other. In the present study, the density of water, lipid and protein were assumed to be 1.00, 0.92, and 1.35 g/cm3, respectively. The mass density for non-calcified arterial plaque is difficult to measure. However, reports have shown that the mass density for myocardial tissue is approximately 1.05 g/cm3 [36]. Thus, the constant volume assumption is expected to be valid here. In fact, our previous study on postmortem breast tissue suggested a good accuracy in three-material decomposition using volume conservation. In the case of calcified plaques, Ca has a mass density of 1.55 g/cm3, which is slightly higher than that of soft tissue. However, in the case of non-calcified plaques and considering the small fraction of Ca (<10%), volume conservation can still be used as a first order approximation. A more rigorous method will be using total mass conservation as the additional constraint. A more generalized method for material-deposition in absence of volume conservation is matter of future studies.

This study proposed a possible method for four-material decomposition using dual-energy CT. Besides volume conservation, another constraint must be provided. The additional constraint was based on the presence of a correlation between the fundamental chemical components of water, lipid and protein contents in soft tissue. This indicates that the four variables are not completely independent of each other. It is thus possible to expand the basis materials beyond three. In early studies by Woodard and White [37], fairly strong correlations among the three fundamental components are shown for adipose and muscle tissues. A previous tissue compositional study on postmortem breasts also suggested a strong correlation between water, lipid and protein contents [29]. It is thus expected that such correlation may also exist for vascular plaque lesions, as the soft tissue component of the lesions consist mostly of adipose and fibrous tissue. Presently, the fundamental chemical compositions of arterial plaques and their potential correlations are unknown. In order to verify the proposed model, this study assumed a water-protein correlation based on a previously reported data [29]. It is important to note that the true correlation for arterial plaque, if any, can be very different from that of breast tissue. However, that does not affect the feasibility study of the proposed four-material decomposition method. The water-protein correlation was not used in material decomposition to quantify lesion chemical composition. It was implemented to define the chemical composition of the tested vessels, such as in Trial 2. The results of the study suggested that four-material decomposition can be performed with reasonably good accuracy using dual-energy CT, as long as there is some correlation between the fundamental components in soft tissue.

In fact, the exact correlation may not affect the precision of the simulation results. The main challenge here is not the linear relationship, but the uncertainty in the biological correlation. This issue was addressed by the addition of some uncertainty in the biological correlation between water and protein as the form of Gaussian noise in Trial 3. Comparing the RMSE in Trial 3 to that in Trial 2, where protein fraction is linearly correlated to water fraction without any uncertainty, results of the simulation show that although the RMSE increased when random noise was added to protein volumetric fraction, the overall accuracy for all four materials was well-preserved. Thus, the proposed method can potentially be used for

measurement of plaque composition as long as there is a reasonable correlation between its water and protein contents.

Dual energy material decomposed CT images are expected to have high noise. It should be noted that the proposed technique is intended to provide quantitative information regarding the chemical composition for the whole plaque. The numerical results, integrated over the whole plaque, may be used as an adjunctive approach to facilitate the conventional image-based diagnosis. A measurement with reasonable accuracy can only be performed using integrated information from relatively large number of voxels, which may be achieved by exploring the whole plaque.

The accuracy of dual-energy material decomposition for four different materials is particularly limited in the case of low attenuation coefficient materials as expected. The accuracy of dual - energy material decomposition is dependent on the ratio of the low and high energy attenuation coefficients and the CT number accuracy. CT number accuracy is dependent on many factors such as beam hardening, scatter, and partial volume effect [38, 39]. These factors should be addressed in order to have the most accurate CT numbers for dual-energy material decomposition. Given the existing beam hardening and scatter correction algorithms, the error in dual-energy material decomposition is expected to be relatively small. However, this error can be much more significant in the case where the ratio of low and high energy attenuation coefficients is small.

The error in dual- energy material decomposition is also dependent on the vessel size. The results of this study showed that the error increased as the vessel size decreased. For example, the RMSEs for water, lipid and protein in a vessel with a 2 mm diameter were approximately 40% higher than in a 5 mm diameter vessel. It was also shown that the error for higher Z materials, such as calcium, is not very sensitive to the change in vessel size. This is due to the fact that the attenuation coefficient of the calcium is higher than that of water, lipid and protein.

In order to investigate the location dependent error in material decomposition, simulation measurements were made both in the right and left side of the heart. The results showed that the decomposition results of the left and right vessels had a good agreement, which means our decomposition study was location independent.

However, there are some limitations in the study. First, the biological correlation used was cited for breast glandular tissue instead of the coronary arterial plaque tissue. This correlation may not accurately translate to other tissues, especially for coronary plaques. This relationship will have to be validated for coronary plaque tissue in future studies. Furthermore, while the vessels investigated in this study were in the range of 2– 5 mm, the plaque size can be smaller than 2 mm, as it may not cover the whole vessel. Therefore, smaller vessel sizes should be considered in future. Finally, the simulation was conducted in an ideal condition where x-ray scatter and beam hardening effects were not included. The simulated CT images are free of artifacts induced by such non-linear effects. The purpose of this simulation study was to determine whether three or four element decomposition is possible assuming that appropriate corrections are made for beam hardening and scatter. CT

manufacturers currently apply corrections for beam hardening and scatter so the next step will be to evaluate the technique using physical phantoms and determine whether further corrections are necessary. This will be done as part of future studies. It is possible to improve the separation of the low and high energy spectra by using Cu or Sn to filter the high energy beam.

In conclusion, the results of this study suggest that the water, lipid, protein, and calcium contents can be accurately measured using dual-energy CT. This technique can potentially be used for quantification of arterial plaque composition.

Acknowledgements

The authors would like to thank Mr. Logan Hubbard for the useful discussion. This work was supported in part by NIH/NCI Grant No. R01CA13687.

References

1. Ren L, Rajendran K, McCollough CH, Yu L. Quantitative accuracy and dose efficiency of dual-contrast imaging using dual-energy CT: a phantom study. Med Phys 2020; 47: 441–56. [PubMed: 31705664]
2. McCollough CH, Boedeker K, Cody D et al. Principles and applications of multienergy CT: Report of AAPM Task Group 291. Med Phys 2020.
3. Gronberg F, Lundberg J, Sjolin M et al. Feasibility of unconstrained three-material decomposition: imaging an excised human heart using a prototype silicon photon-counting CT detector. Eur Radiol 2020.
4. Zhao W, Vernekohl D, Han F et al. A unified material decomposition framework for quantitative dual- and triple-energy CT imaging. Med Phys 2018; 45: 2964–77. [PubMed: 29679500]
5. Raja AY, Moghiseh M, Bateman CJ et al. Measuring Identification and Quantification Errors in Spectral CT Material Decomposition. Appl Sci-Basel 2018; 8.
6. De Santis D, Eid M, De Cecco CN et al. Dual-Energy Computed Tomography in Cardiothoracic Vascular Imaging. Radiol Clin N Am 2018; 56: 521–+. [PubMed: 29936945]
7. Machida H, Tanaka I, Fukui R et al. Dual-Energy Spectral CT: Various Clinical Vascular Applications. Radiographics 2016; 36: 1215–32. [PubMed: 27399244]
8. Alvarez RE, Macovski A. Energy-Selective Reconstructions in X-Ray Computerized Tomography. Physics in Medicine and Biology 1976; 21: 733–44. [PubMed: 967922]
9. Lehmann LA, Alvarez RE, Macovski A et al. Generalized image combinations in dual KVP digital radiography. Med Phys 1981; 8: 659–67. [PubMed: 7290019]
10. Tran DN, Straka M, Roos JE et al. Dual-energy CT Discrimination of Iodine and Calcium: Experimental Results and Implications for Lower Extremity CT Angiography. Academic Radiology 2009; 16: 160–71. [PubMed: 19124101]
11. Gupta R, Phan CM, Leidecker C et al. Evaluation of Dual-Energy CT for Differentiating Intracerebral Hemorrhage from Iodinated Contrast Material Staining. Radiology 2010; 257: 205–11. [PubMed: 20679449]
12. Hubbell JH, Seltzer SM. Tables of x-ray mass attenuation coeeficient and mass energy absorption coefficients 1 keV to 20 MeV for elements Z=1 to 92 and 48 additional substances of dosimetric interest. NIST Report No NISTIR 5632 1995.
13. Liu X, Yu LF, Primak AN, McCollough CH. Quantitative imaging of element composition and mass fraction using dual-energy CT: Three-material decomposition. Med Phys 2009; 36: 1602–9. [PubMed: 19544776]
14. Johnson TRC, Krauss B, Sedlmair M et al. Material differentiation by dual energy CT: initial experience. Eur Radiol 2007; 17: 1510–7. [PubMed: 17151859]

15. Obaid DR, Calvert PA, Gopalan D et al. Dual-energy computed tomography imaging to determine atherosclerotic plaque composition: A prospective study with tissue validation. J Cardiovasc Comput 2014; 8: 230–7.
16. Mandal SR, Bharati A, Haghighi RR et al. Non-invasive characterization of coronary artery atherosclerotic plaque using dual energy CT: Explanation in ex-vivo samples. Physica Medica-European Journal of Medical Physics 2018; 45: 52–8.
17. Sangiorgi G, Rumberger JA, Severson A et al. Arterial calcification and not lumen stenosis is highly correlated with atherosclerotic plaque burden in humans: a histologic study of 723 coronary artery segments using nondecalcifying methodology. Journal of the American College of Cardiology 1998; 31: 126–33. [PubMed: 9426030]
18. Kuhnigk JM, Dicken V, Bornemann L et al. Morphological segmentation and partial volume analysis for volumetry of solid pulmonary lesions in thoracic CT scans. Ieee Transactions on Medical Imaging 2006; 25: 417–34. [PubMed: 16608058]
19. Schaar JA, Muller JE, Falk E et al. Terminology for high-risk and vulnerable coronary artery plaques. Report of a meeting on the vulnerable plaque, June 17 and 18, 2003, Santorini, Greece. Eur Heart J 2004; 25: 1077–82. [PubMed: 15191780]
20. Arbab-Zadeh A, Fuster V. The myth of the “vulnerable plaque”: transitioning from a focus on individual lesions to atherosclerotic disease burden for coronary artery disease risk assessment. Journal of the American College of Cardiology 2015; 65: 846–55. [PubMed: 25601032]
21. Johri AM, Nambi V, Naqvi TZ et al. Recommendations for the Assessment of Carotid Arterial Plaque by Ultrasound for the Characterization of Atherosclerosis and Evaluation of Cardiovascular Risk: From the American Society of Echocardiography. J Am Soc Echocardiogr 2020.
22. Ding H, Ducote JL, Molloi S. Breast composition measurement with a cadmium-zinc-telluride based spectral computed tomography system. Med Phys 2012; 39: 1289–97. [PubMed: 22380361]
23. Li Z, Leng S, Yu L et al. Image-based Material Decomposition with a General Volume Constraint for Photon-Counting CT. Proc SPIE Int Soc Opt Eng 2015; 9412.
24. Lee SW, Choi YN, Kim HJ. Quantitative material decomposition using spectral computed tomography with an energy-resolved photon-counting detector. Physics in Medicine and Biology 2014; 59: 5457–82. [PubMed: 25164993]
25. Badea CT, Holbrook M, Clark DP, Ghaghada K. Spectral Imaging of Iodine and Gadolinium Nanoparticles Using Dual-Energy CT. Medical Imaging 2018: Physics of Medical Imaging 2018; 10573.
26. Goodsitt MM, Rosenthal DI. Quantitative Computed-Tomography Scanning for Measurement of Bone and Bone-Marrow Fat-Content - a Comparison of Single-Energy and Dual-Energy Techniques Using a Solid Synthetic Phantom. Invest Radiol 1987; 22: 799–810. [PubMed: 3429176]
27. Nowotny R, Hofer A. [Program for calculating diagnostic x-ray spectra]. Rofo 1985; 142: 685–9. [PubMed: 2988070]
28. van Aarle W, Palenstijn WJ, De Beenhouwer J et al. The ASTRA Toolbox: A platform for advanced algorithm development in electron tomography. Ultramicroscopy 2015; 157: 35–47. [PubMed: 26057688]
29. Johnson T, Ding H, Molloi S. Breast density quantification with breast computed tomography (CT): A post-mortem study. Physics in Medicine and Biology 2013; 58: 8573–91. [PubMed: 24254317]
30. Achenbach S, Moselewski F, Ropers D et al. Detection of calcified and noncalcified coronary atherosclerotic plaque by contrast-enhanced, submillimeter multidetector spiral computed tomography - A segment-based comparison with intravascular ultrasound. Circulation 2004; 109: 14–7. [PubMed: 14691045]
31. Hoffmann U, Moselewski F, Nieman K et al. Noninvasive assessment of plaque morphology and composition in culprit and stable lesions in acute coronary syndrome and stable lesions in stable angina by multidetector computed tomography. Journal of the American College of Cardiology 2006; 47: 1655–62. [PubMed: 16631006]

32. Leber AW, Knez A, White CW et al. Composition of coronary atherosclerotic plaques in patients with acute myocardial infarction and stable angina pectoris determined by contrast-enhanced multislice computed tomography. Am J Cardiol 2003; 91: 714–8. [PubMed: 12633805]

33. Earls JP, Berman EL, Urban BA et al. Prospectively gated transverse coronary CT angiography versus retrospectively gated helical technique: Improved image quality and reduced radiation dose. Radiology 2008; 246: 742–53. [PubMed: 18195386]

34. Raff GL, Gallagher MJ, O'Neill W, Goldstein JA. Diagnostic accuracy of noninvasive coronary angiography using 64-slice spiral computed tomography. Journal of the American College of Cardiology 2005; 46: 552–7. [PubMed: 16053973]

35. Ding H, Klopfer MJ, Ducote JL et al. Breast Tissue Characterization with Photon-counting Spectral CT Imaging: A Postmortem Breast Study. Radiology 2014; 272: 731–8. [PubMed: 24814180]

36. Vinnakota KC, Bassingthwaighte JB. Myocardial density and composition: a basis for calculating intracellular metabolite concentrations. Am J Physiol-Heart C 2004; 286: H1742–H9.

37. Woodard HQ, White DR. The Composition of Body-Tissues. British Journal of Radiology 1986; 59: 1209–19.

38. McCollough CH, Zink FE, Welch TJ. Performance evaluation of a multi-slice CT system. Radiology 1999; 210: 586–.

39. Kopp AF, Ohnesorge B, Becker C et al. Reproducibility and accuracy of coronary calcium measurements with multi-detector row versus electron-beam CT. Radiology 2002; 225: 113–9. [PubMed: 12354993]

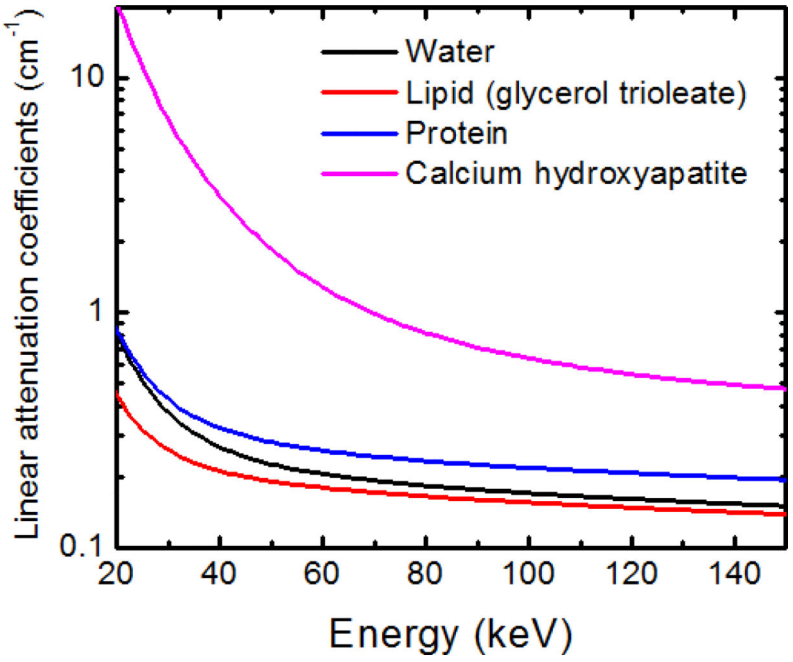

Figure 1.

Mass attenuation coefficient in the logarithmic coordinate for the four materials considered in this study within the diagnostic energy range.

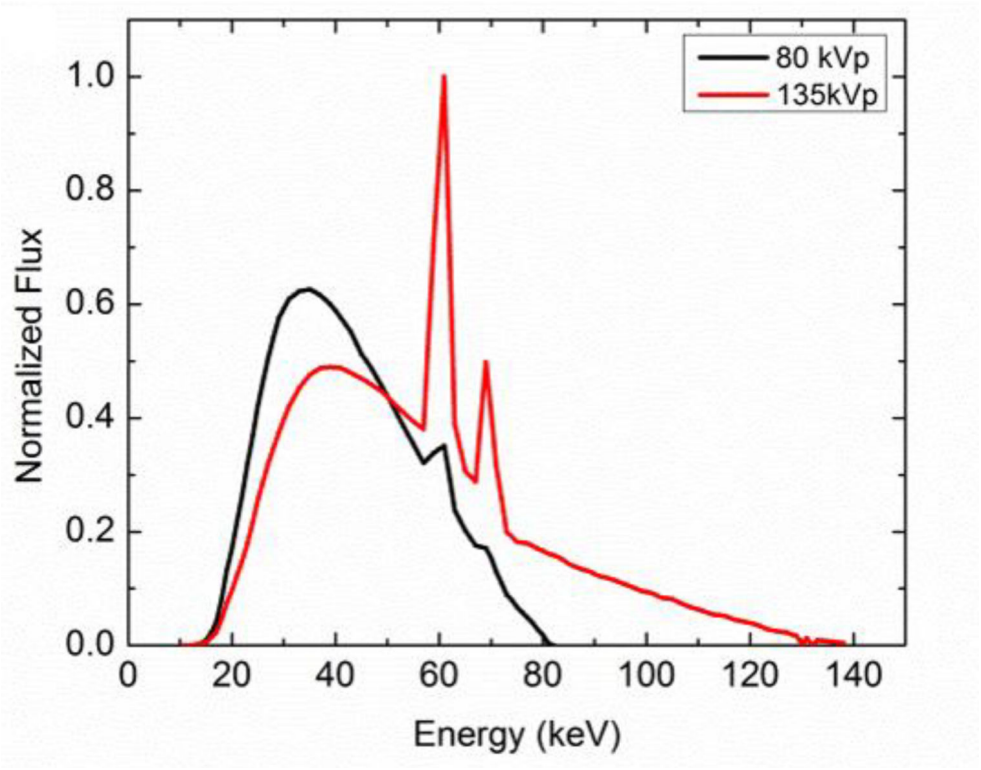

Figure 2.
Polyenergetic x-ray beam flux at 80 and 135 kVp tube voltages.

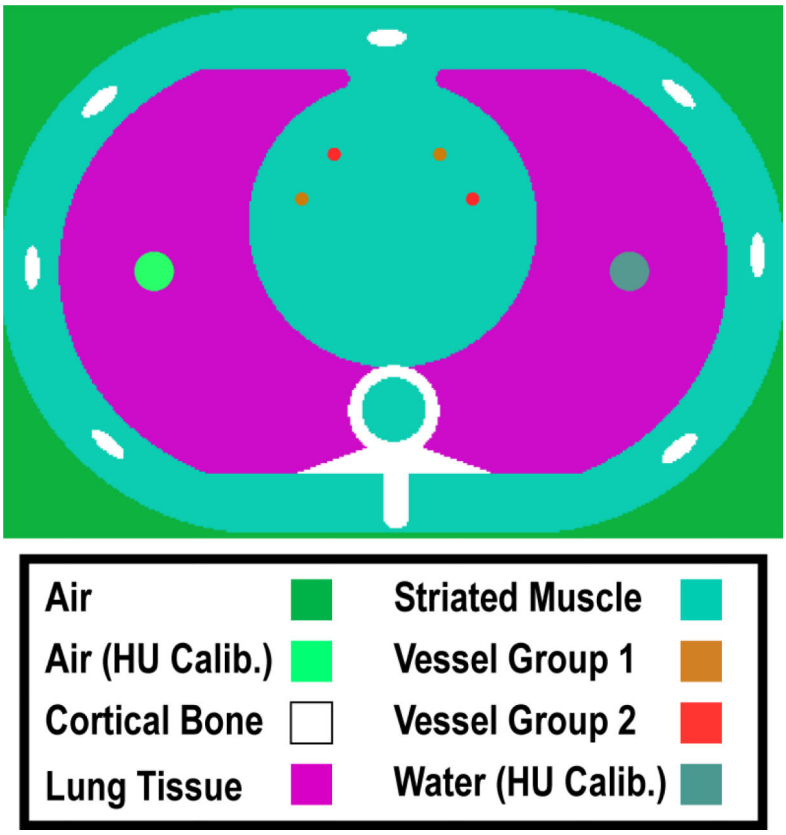

Figure 3.
Chest image phantom used in the dual energy CT simulation. Different colored vessels stand for different materials.

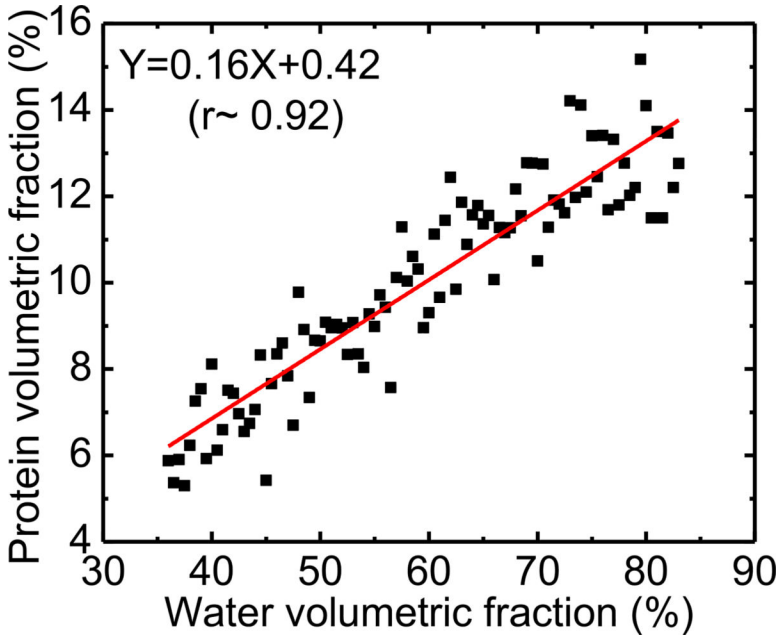

Figure 4.
Correlation of volumetric fraction of water and protein in the soft human tissue experimental data with Gaussian noise introduced. The red line is the linear fitting line of the original data.

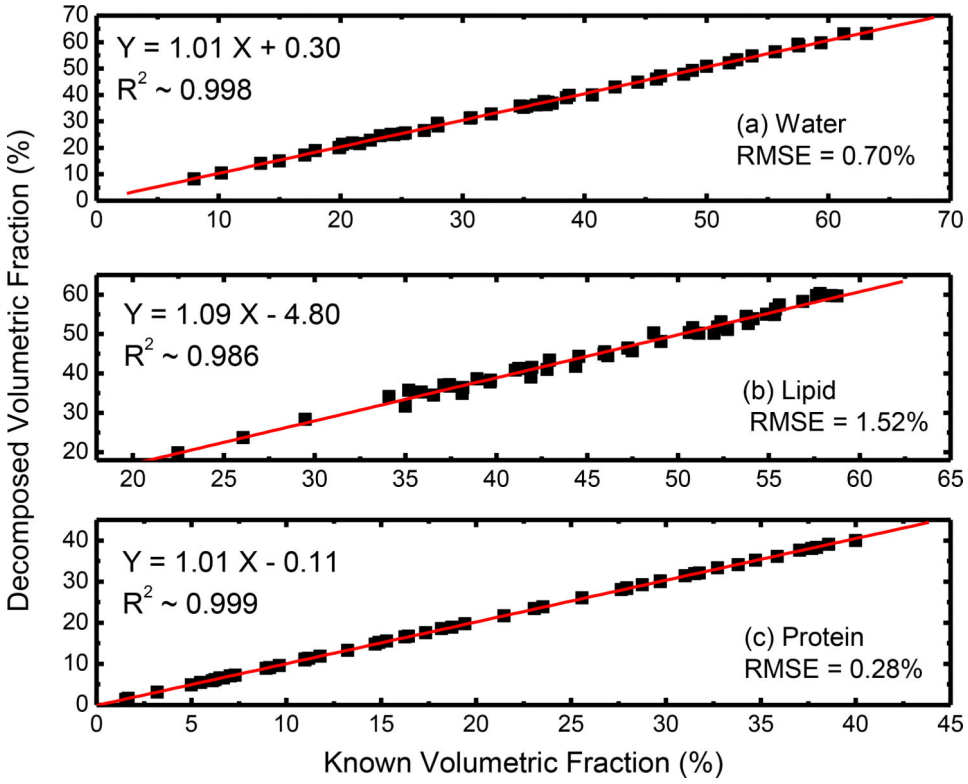

Figure 5.

Results of the three-material mixture compositional studies of trial 1. The volumetric fractions of water (a), lipid (b), and protein (c) contents measured with dual kVp technique are presented as a function of the designed phantom. The Y axes are the dual-energy decomposition volumetric fractions of water, lipid, and protein. Identity lines are drawn for visual guidance. Excellent correlations with slopes very close to one can be observed for all three contents.

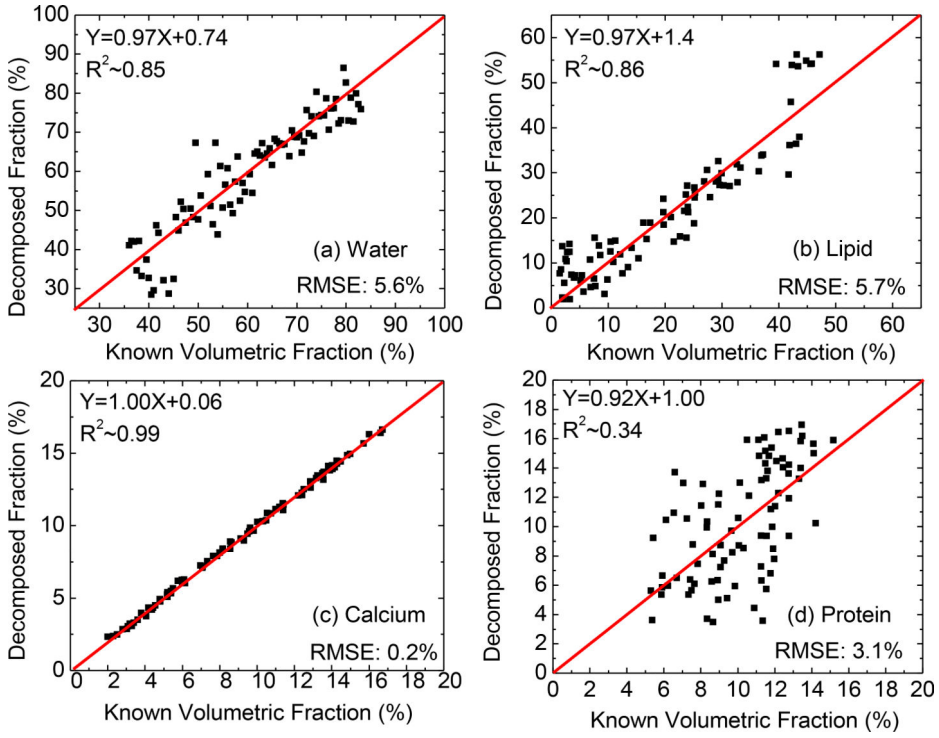

Figure 6.

Results of the four-material mixture compositional studies of trial 3. The volumetric fractions of water (a), lipid (b), calcium (c), and protein (d) contents measured with dual kVp technique are presented as a function of the known volumetric fractions. Identity lines are drawn for visual guidance. Excellent correlations with slopes close to one can be observed for all contents.

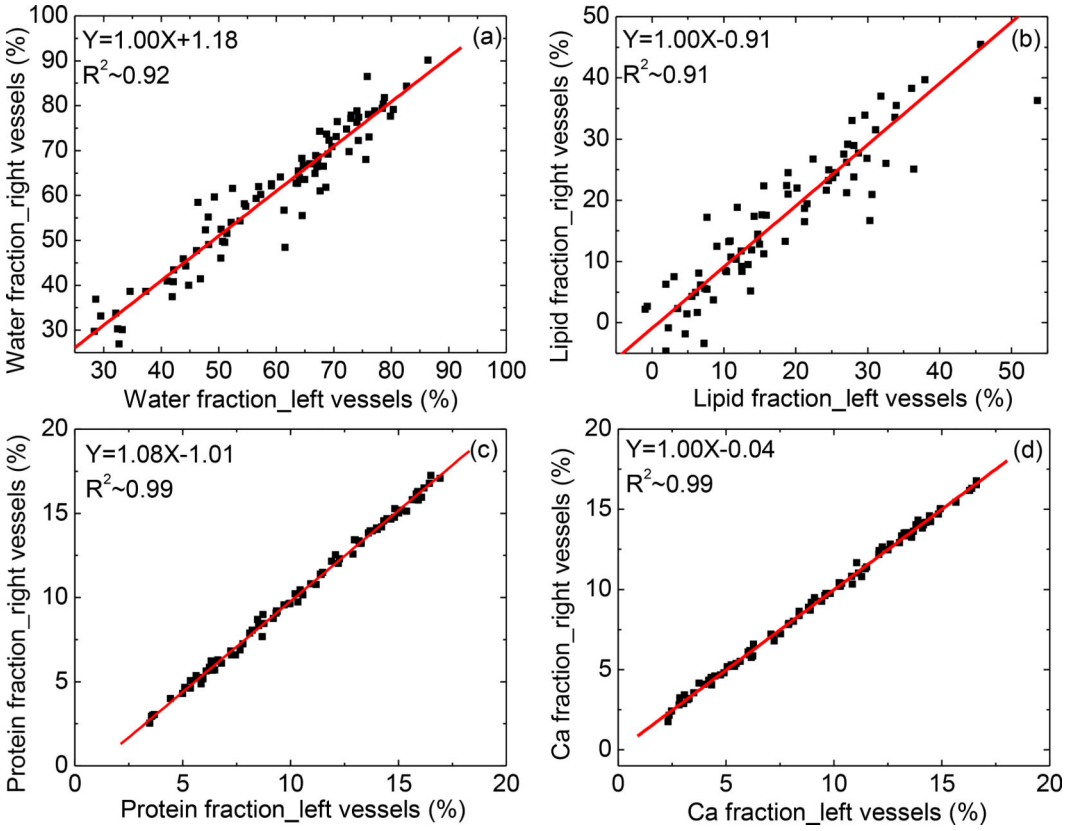

Figure 7.

Correlation between the left and the right vessels of the simulation compositional studies of trial 3. The same mixtures were simulated simultaneously on both sides of the heart. The volumetric fractions of water (a), lipid (b), protein (c), and calcium (d) contents measured with dual kVp technique are presented for the results on both sides. In all cases, the slopes are close to one, which suggests the decomposition accuracy is independent of the vessel position.

Table 1.

Simulation parameters which matched the specification of Canon Aquilion One CT scanner.

Canon Aquilion One Specifications	
X-ray Source Filtration	7.5 mm Al
Detector Pixel Pitch	0.5 mm
Number of Projection Angles	900
Source to Object Distance	60.0 cm
Object to Detector Distance	47.2 cm
Focal Spot Size	0.9 mm

Table 2.

Plaque composition information from the literature and composition used in simulation studies.

	Non-calcified (literature) (%)	Non-calcified (simulation) (%)	Calcified (literature) (%)	Calcified (simulation) (%)
water	50–90	35–65	36–83	36–83
lipid	3.7–36	5–60	8.6–34.6	1.7–47.2
protein	6.2–15.4	5–40	5.2–13.6	5.2–15.2
calcium			3–17	2–17

Table 3.

The specifications for each trial. W, L, P, and Ca stand for water, Lipid, Protein, and Calcium, respectively.

	Diameter (mm)	Biological Uncertainty	Exposure	Composition (W, L, P, Ca)
Trial 1	2	w/	0.5	W, L, P
Trial 2	5	w/o	0.5	W, L, P, Ca
Trial 3	5	w/	0.5	W, L, P, Ca
Trial 4	3	w/	0.5	W, L, P, Ca
Trial 5	2	w/	0.5	W, L, P, Ca

Table 4.

The RMSE statistical analysis results for all dual kVp CT simulation decomposition trials. The range of all contents is shown at the bottom for reference.

RMSE	Water (%)	Lipid (%)	Calcium (%)	Protein (%)
Trial 1	3.16	2.08	N/A	0.23
Trial 2	2.88	4.23	0.59	2.02
Trial 3	4.19	4.6	0.57	1.86
Trial 4	6.22	7.19	0.67	2.30
Trial 5	5.76	6.86	0.68	2.41
Range	36–83	1.7–41.2	2–16.8	5.3–15.2

Table 5.

The SEE statistical analysis results for all dual kVp CT simulation decomposition trials. The range of all contents is shown at the bottom for reference.

SEE	Water (%)	Lipid (%)	Calcium (%)	Protein (%)
Trial 1	0.55	1.15	N/A	0.17
Trial 2	5.37	5.02	0.20	3.15
Trial 3	5.54	5.57	0.17	3.13
Trial 4	6.55	6.93	0.36	3.01
Trial 5	8.05	7.43	0.43	2.72
Range	36–83	1.7–41.2	2–16.8	5.3–15.2